AIAA JOURNAL
Vol. 41, No. 12, December 2003

Analysis of Locally Irregular Composites Using High-Fidelity Generalized Method of Cells

Marek-Jerzy Pindera*
University of Virginia, Charlottesville, Virginia 22904
Jacob Aboudi†
Tel-Aviv University, 69978 Ramat-Aviv, Israel
and
Steven M. Arnold‡
NASA John H. Glenn Research Center at Lewis Field, Cleveland, Ohio 44135

The generalized method of cells is a micromechanics model that is generally quite accurate at the macrolevel but not always accurate at the microlevel. This is due to the absence of so-called shear coupling, which provides the required bridge between macroscopically applied normal (shear) stresses and the microscopic shear (normal) stresses necessary for an accurate estimate of microlevel quantities. To overcome this deficiency, a new micromechanics model has been developed for the response of multiphase materials with arbitrary periodic microstructures, named high-fidelity generalized method of cells in part because it employs the same microstructural discretization as the original generalized method of cells. The model's framework is based on the homogenization theory, but the method of solution for the local fields borrows concepts previously employed in constructing the higher-order theory for functionally graded materials, in contrast with the typical finite element-based solution strategies. The model generates the average stress–strain response of heterogeneous materials such as ceramic, metal, and polymeric matrix composites, as well as the internal or microlevel stress and strain fields, with excellent accuracy. The model is employed to investigate the response of a metal matrix composite with locally irregular, but periodic, fiber distributions, and it is shown that irregular architectures affect shear and normal stress–strain response in a different manner. The new model's ability to capture these differences is attributed to the shear-coupling effect absent in the original model.

Nomenclature

$\boldsymbol{A}^{(\beta\gamma)}$	=	Hill's[1] elastic strain concentration matrix for the $(\beta\gamma)$ subcell
$\boldsymbol{C}^*$	=	effective stiffness matrix of the composite material
$\boldsymbol{D}^{(\beta\gamma)}$	=	thermoplastic effect vector for the $(\beta\gamma)$ subcell
$d\bar{\varepsilon}^p$	=	effective plastic strain increment
$d\varepsilon_{ij}^p$	=	plastic strain increments
E, E_s	=	Young's modulus and secondary modulus
e'_{ij}	=	Mendelson's[10] modified total strain deviators
$\boldsymbol{f}, \boldsymbol{g}$	=	thermomechanical and plastic force vectors for the repeating unit cell
H, L	=	dimensions of the repeating unit cell
H_p	=	slope of the effective stress-plastic strain curve
$h_\beta^{(q)}, l_\gamma^{(r)}$	=	dimensions of the $(\beta\gamma)$ subcell in the (q, r) cell
$\boldsymbol{K}$	=	structural stiffness matrix for the repeating unit cell
$P_m(\cdot)$	=	Legendre polynomial of order m
$R_{ij(m,n)}^{(\beta\gamma)}$	=	plastic strain distribution components in the subcell $(\beta\gamma)$
$\boldsymbol{U}$	=	displacement vector characterizing the repeating unit cell response
u_i	=	global displacement components
$u_{\alpha i}$	=	different-order terms in the global displacement field expansion
$u_i^{(\beta\gamma)}$	=	displacement components within the $(\beta\gamma)$ subcell
$\bar{u}_i$	=	average displacement components
$\tilde{u}_i$	=	local displacement components
$W_{i(mn)}^{(\beta\gamma)}$	=	microvariables in the displacement field approximation within the $(\beta\gamma)$ subcell
x_i	=	macroscopic coordinates
y_i	=	microscopic coordinates
$\bar{y}_2^{(\beta)}, \bar{y}_3^{(\gamma)}$	=	local subcell coordinates
$\boldsymbol{\Gamma}^{(\beta\gamma)}$	=	thermal stress tensor of the material in the $(\beta\gamma)$ subcell
$\varepsilon_{kl}^{p(\beta\gamma)}$	=	plastic strains in the $(\beta\gamma)$ subcell
$\bar{\varepsilon}_{ij}$	=	average composite strains
$\tilde{\varepsilon}_{ij}$	=	local composite strains
$\bar{\varepsilon}^{(\beta\gamma)}$	=	average total strains in the $(\beta\gamma)$ subcell
$\zeta_i^{(\cdot)}$	=	nondimensionalized subcell coordinates
μ	=	shear modulus
σ_y	=	yield stress in pure tension
$\bar{\boldsymbol{\sigma}}, \bar{\boldsymbol{\sigma}}^I, \bar{\boldsymbol{\sigma}}^T$	=	composite total, inelastic, and thermal stresses
$\bar{\sigma}_{\text{eff}}$	=	effective stress

Presented as Paper 2003-1918 at the AIAA/ASME/ASCE/AHS/ASC 44th Structures, Structural Dynamics, and Materials Conference, Norfolk, Virginia, 7–10 April 2003; received 4 June 2003; revision received 28 July 2003; accepted for publication 29 July 2003.

*Professor, Department of Civil Engineering.
†Professor, Department of Solids Mechanics, Materials and Structures.
‡Senior Research Engineer, Structural Fatigue Branch.

Introduction

MICROMECHANICAL modeling techniques are important tools in many advanced applications that require the use of engineered microstructures involving multiphase material concepts. They make it possible to analyze efficiently how different microstructural details affect the average and local responses of multiphase materials in the quest to develop optimum material architectures for specific applications.

Micromechanical techniques for the response of heterogeneous materials developed during the past several decades include simple Voigt and Reuss hypotheses, self-consistent schemes and their generalizations, differential schemes, concentric cylinder models,

bounding techniques, and approximate or numerical analyses of periodic arrays of inclusions or fibers in the surrounding matrix phase. These approaches may be divided into three broad categories: those based on the direct calculation of Hill's stress or strain concentration matrices[1] developed for two-phase composites and those based on the concepts of a representative volume element (RVE) and a repeating unit cell (RUC). RVE-based approaches employ simplified geometric representations of the entire composite for which analytical solutions under homogeneous displacement or traction boundary conditions are readily available. Therefore, they are not suitable for the analysis of periodic composites with locally irregular microstructures. RUC-based approaches, on the other hand, model the actual microstructure of a material's subvolume which is assumed to repeat itself, and, therefore, often rely on numerical solutions of the governing field equations using finite difference or finite element methods. Symmetry boundary conditions are typically employed in those situations where the RUC possesses material symmetry that is retained in the deformed state. Periodic boundary conditions must be applied to the RUC in the absence of material symmetry or symmetry-preserving loading.

The use of periodic boundary conditions together with a multiscale asymptotic representation of the displacement field within an RUC forms the basis of the homogenization theory for estimating the effective response of periodic materials. This theory is particularly effective when applied to periodic multiphase materials that are characterized by an arbitrary distribution of different phases within an RUC. In particular, it provides the correct periodic boundary conditions that must be applied to the RUC under loading along different directions,[2] thereby avoiding the need for ad hoc assumptions on the deformation of the RUC's bounding surface under multi-axial loading. However, with the exception of simple RUC architectures amenable to analytical solutions, the simulation of effective response is performed through a numerical analysis of the RUC such as the finite element approach.

To overcome this disadvantage, a new analytical model for the effective response of continuously reinforced, periodic multiphase materials has been developed that circumvents the use of a finite element solution for the displacement and stress fields within an RUC.[3–5] When this approach is used, periodic materials with arbitrary phase distributions in the plane normal to the continuous reinforcement, whose response in this plane is fully anisotropic, can be modeled. The model's analytical framework is based on the homogenization theory, but the method of solution for the local displacement and stress fields within an RUC utilizes concepts previously employed in constructing higher-order theory for functionally graded materials.[6] The homogenization theory is used to construct a higher-order displacement field approximation at the local microstructural level of a periodic multiphase material in a consistent fashion and to derive the governing field equations and the boundary conditions that the displacement field must satisfy. The actual solution for the local displacement and strain and stress fields follows the already mentioned higher-order theory. It is based on discretization of the RUC into rectangular cells that are assigned material properties to mimic the material's periodic microstructure and satisfaction of the field equations in a volumetric, and continuity and periodic boundary conditions in a surface-average, sense. The higher-order displacement field approximation at the local level provides the necessary coupling between the local normal and in-plane shear stress fields and the macroscopically applied loading. This coupling dramatically improves the accuracy of estimating the local stress fields relative to the generalized method of cells,[7] which is based on a first-order displacement approximation at the local level. The new model's name is high-fidelity generalized method of cells (HFGMC) to reflect both the enhanced accuracy and similar volume discretization relative to the original generalized method of cells (GMC).

The HFGMC model's predictive accuracy in generating the effective elastic moduli, inelastic stress–strain response, and the local stress and inelastic strain fields has been demonstrated by comparison with the results of analytical elasticity, plasticity, and finite element solutions involving a circular inclusion in an infinite matrix subjected to a uniform far-field stress, a concentric cylinder subjected to axisymmetric and axial shear loading, and a square fiber array under transverse biaxial tension–compression, respectively.[3–5] These validation studies have been performed for simple microstructures characterized by orthogonal planes of material symmetry. To date, no data have been generated on unidirectional composites with locally irregular microstructures using HFGMC. It is for such composites that the power of HFGMC will become evident due to the importance of shear coupling in the presence of locally irregular microstructures. The differences between the original GMC and the new HFGMC models are also expected to be highlighted in these circumstances.

Note that limited GMC-based analyses of statistically homogeneous (and locally irregular) unidirectional composites have been conducted by Orozco[8] and Orozco and Pindera,[9] where it was demonstrated that correct effective moduli trends were predicted by GMC with increasing microstructural refinement in the elastic region and under certain loading conditions and material symmetries in the inelastic region. However, the impact of the shear coupling's absence on both the macroscopic and microscopic responses could not be investigated thoroughly due to the original GMC model's obvious limitations. This limitation is no longer present in the new HFGMC model, enabling direct assessment of the shear coupling's influence on the response of both regular and locally irregular periodic composites through comparison of the two model's predictive capabilities.

In the present paper, therefore, HFGMC is employed to analyze the effective response and local stress fields in unidirectional metal matrix composites with periodic, but locally irregular, fiber distributions. Of particular interest is the effect of local fiber distribution inhomogeneity on the effective response in the plane perpendicular to the fiber direction relative to the effective response of a composite with regular (square) fiber distribution. Two types of irregular fiber architectures are considered, one of which produces monoclinic symmetry. These fiber architectures cannot be analyzed reliably using the original GMC due to the absence of shear coupling responsible for the observed differences predicted by the new model. This is highlighted through comparison of the two models' predictions of such composites' macroscopic and microscopic responses.

Analytical Foundations of HFGMC

The theoretical framework of HFGMC has been well documented by Aboudi et al.,[3–5] and therefore, only a brief outline will be presented here to facilitate correct interpretation of the results that follow. Consider a multiphase composite with a periodic microstructure in the $x_2 - x_3$ plane shown in Fig. 1, where the repeating unit cell used to construct the periodic array is highlighted. In the framework of the homogenization theory, the displacement field is represented by the two-scale expansion

$$u_i(x, y) = u_{i0}(x, y) + \delta u_{i1}(x, y) + \delta^2 u_{i2}(x, y) + \cdots \qquad (1)$$

where $x = (x_1, x_2, x_3)$ are the macroscopic coordinates, $y = (y_1, y_2, y_3)$ are the microscopic coordinates defined with respect to

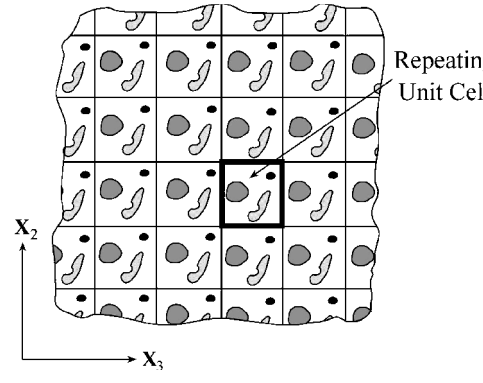

Fig. 1 Multiphase material with a periodic microstructure in the transverse plane characterized by an RUC.

the repeating unit cell, and the different-order terms in the displacement field expansion are y periodic due to the material's periodicity. The size of the repeating unit cell characterized by the parameter δ is considered small relative to the overall material dimensions such that $y_i = x_i/\delta$, which implies that a unit displacement at the local scale corresponds to a small displacement on the global scale.

The preceding displacement field representation, in conjunction with the relation between the two scales, allows us to express the strain field in periodic composites in terms of the average and fluctuating strain quantities, $\bar{\varepsilon}_{ij}(x)$ and $\tilde{\varepsilon}_{ij}(x, y)$, respectively,

$$\varepsilon_{ij} = \bar{\varepsilon}_{ij}(x) + \tilde{\varepsilon}_{ij}(x, y) + \mathcal{O}(\delta) \tag{2}$$

where the average and fluctuating (local) strains are given in terms of the corresponding displacements $\bar{u}_i$ and $\tilde{u}_i$,

$$\bar{\varepsilon}_{ij}(x) = \frac{1}{2}\left(\frac{\partial \bar{u}_i}{\partial x_j} + \frac{\partial \bar{u}_j}{\partial x_i}\right), \qquad \tilde{\varepsilon}_{ij}(x, y) = \frac{1}{2}\left(\frac{\partial \tilde{u}_i}{\partial y_j} + \frac{\partial \tilde{u}_j}{\partial y_i}\right) \tag{3}$$

The preceding strain decomposition makes it possible to express the displacement field in the form

$$u_i(x, y) = \bar{\varepsilon}_{ij} x_j + \tilde{u}_i + \mathcal{O}(\delta^2) \tag{4}$$

which is employed in constructing an approximate displacement field for the solution of the cell problem discussed in the sequel.

For specified values of the average strains, the unknown fluctuating displacements are governed by the equilibrium equations subject to periodic boundary conditions imposed on the displacement and traction components that are prescribed at the boundaries of the RUC. In addition to these boundary conditions, one needs to impose the continuity of displacements and tractions at the internal interfaces between the phases that fill the RUC. The manner of solving the governing field equations for the fluctuating displacements in the RUC based on the already given representation is described next.

Cell Problem

The local analysis is performed on the RUC, appropriately discretized into generic cells and subcells to mimic the material's periodic microstructure, as shown in Fig. 2 for the RUC highlighted in Fig. 1. The indices q and r, whose ranges are $q = 1, \ldots, N_q$ and $r = 1, \ldots, N_r$, identify the generic cell (or the basic building block of the RUC) in the $y_2 - y_3$ plane. The dimensions of the generic cell

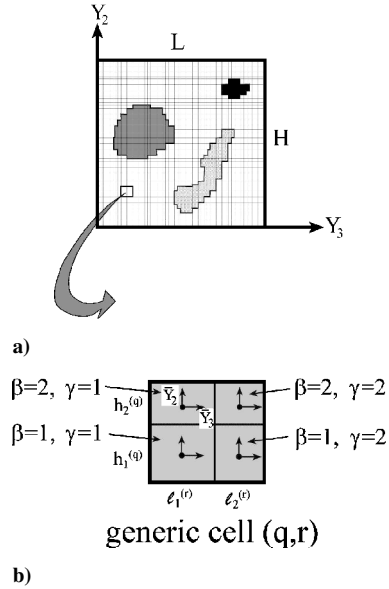

Fig. 2 RUC from Fig. 1: a) volume discretization and b) generic cell within RUC.

along the y_2 and y_3 axes are $h_1^{(q)}, h_2^{(q)}$ and $l_1^{(r)}, l_2^{(r)}$, respectively, such that

$$H = \sum_{1}^{N_q} \left(h_1^{(q)} + h_2^{(q)}\right), \qquad L = \sum_{1}^{N_r} \left(l_1^{(r)} + l_2^{(r)}\right) \tag{5}$$

Following the general displacement field representation for periodic media based on the two-scale expansion technique, the subcell displacement field approximation has the following form, omitting the cell label (q, r):

$$u_1^{(\beta\gamma)} = \bar{\varepsilon}_{1j} x_j + W_{1(00)}^{(\beta\gamma)} + \bar{y}_2^{(\beta)} W_{1(10)}^{(\beta\gamma)} + \bar{y}_3^{(\gamma)} W_{1(01)}^{(\beta\gamma)} + \tfrac{1}{2}\left(3\bar{y}_2^{(\beta)2} - h_\beta^{(q)2}/4\right) W_{1(20)}^{(\beta\gamma)} + \tfrac{1}{2}\left(3\bar{y}_3^{(\gamma)2} - l_\gamma^{(r)2}/4\right) W_{1(02)}^{(\beta\gamma)} \tag{6}$$

$$u_2^{(\beta\gamma)} = \bar{\varepsilon}_{2j} x_j + W_{2(00)}^{(\beta\gamma)} + \bar{y}_2^{(\beta)} W_{2(10)}^{(\beta\gamma)} + \bar{y}_3^{(\gamma)} W_{2(01)}^{(\beta\gamma)} + \tfrac{1}{2}\left(3\bar{y}_2^{(\beta)2} - h_\beta^{(q)2}/4\right) W_{2(20)}^{(\beta\gamma)} + \tfrac{1}{2}\left(3\bar{y}_3^{(\gamma)2} - l_\gamma^{(r)2}/4\right) W_{2(02)}^{(\beta\gamma)} \tag{7}$$

$$u_3^{(\beta\gamma)} = \bar{\varepsilon}_{3j} x_j + W_{3(00)}^{(\beta\gamma)} + \bar{y}_2^{(\beta)} W_{3(10)}^{(\beta\gamma)} + \bar{y}_3^{(\gamma)} W_{3(01)}^{(\beta\gamma)} + \tfrac{1}{2}\left(3\bar{y}_2^{(\beta)2} - h_\beta^{(q)2}/4\right) W_{3(20)}^{(\beta\gamma)} + \tfrac{1}{2}\left(3\bar{y}_3^{(\gamma)2} - l_\gamma^{(r)2}/4\right) W_{3(02)}^{(\beta\gamma)} \tag{8}$$

The unknown microvariables $W_{i(mn)}^{(\beta\gamma)}$ in the fluctuating part of the subcell displacement field representation are determined by satisfying the equilibrium equations in the subcell $(\beta\gamma)$ in a volumetric sense and the displacement and traction continuity conditions between subcells within a generic cell, and between adjacent generic cells, in a surface-average sense. In addition, the periodic boundary conditions are imposed in a surface-averaged sense as well. Application of the preceding equations and conditions in this manner produces a system of $60N_qN_r$ algebraic equations in the unknown coefficients $W_{i(mn)}^{(\beta\gamma)}$ of the form

$$\boldsymbol{K}\boldsymbol{U} = \boldsymbol{f} + \boldsymbol{g} \tag{9}$$

where the structural stiffness matrix $\boldsymbol{K}$ contains information on the geometry and thermomechanical properties of the individual subcells $(\beta\gamma)$ within the cells comprising the multiphase periodic composite. The displacement coefficient vector $\boldsymbol{U}$ contains the unknown coefficients that describe the displacement field in each subcell, that is,

$$\boldsymbol{U} = \left[\boldsymbol{U}_{11}^{(11)}, \ldots, \boldsymbol{U}_{N_qN_r}^{(22)}\right] \tag{10}$$

where $U_{qr}^{(\beta\gamma)} = [W_{i(00)}, W_{i(10)}, W_{i(01),} W_{i(20)}, W_{i(02)}]_{qr}^{(\beta\gamma)}$ and the mechanical force vector $\boldsymbol{f}$ contains information on the applied average strains and the imposed spatially uniform temperature change. In addition, the inelastic force vector $\boldsymbol{g}$ appearing on the right-hand side of the global system of equations contains inelastic effects given in terms of the integrals of the plastic strain distributions $\varepsilon_{kl}^{p(\beta\gamma)}(\bar{y}_2^{(\beta)}, \bar{y}_3^{(\gamma)})$ that are represented by the coefficients $R_{ij(m,n)}^{(\beta\gamma)}$,

$$R_{ij(m,n)}^{(\beta\gamma)} = \frac{1}{2}\mu^{(\beta\gamma)}\sqrt{(2m+1)(2n+1)} \times \int_{-1}^{+1}\int_{-1}^{+1} \varepsilon_{ij}^{p(\beta\gamma)} P_m\left(\zeta_2^{(\beta)}\right) P_n\left(\zeta_3^{(\gamma)}\right) \mathrm{d}\zeta_2^{(\beta)}\, \mathrm{d}\zeta_3^{(\gamma)} \tag{11}$$

where the nondimensionalized variables $\zeta_i^{(\cdot)}$, defined in the interval $-1 \le \zeta_i^{(\cdot)} \le 1$, are given in terms of the local subcell coordinates $\zeta_2^{(\beta)} = \bar{y}_2^{(\beta)}/(h_\beta^{(q)}/2)$ and $\zeta_3^{(\gamma)} = \bar{y}_3^{(\gamma)}/(l_\gamma^{(r)}/2)$, and where $P_m(\cdot)$ and $P_n(\cdot)$ are Legendre polynomials of order m and n. These integrals depend implicitly on the elements of the displacement coefficient vector $\boldsymbol{U}$, requiring an incremental solution of the global equations

at each point along the loading path. The outlined formulation is sufficiently general to admit either rate-independent incremental plasticity, rate-dependent creep, or unified viscoplasticity constitutive theories.

Homogenized Constitutive Equations

The solution for the displacement vector $\boldsymbol{U}$ containing the unknown subcells microvariables $W_{i(mn)}^{(\beta\gamma)}$ in terms of the applied average strain $\bar{\varepsilon}$ enables the determination of the localization relations. These are given in terms of so-called Hill's strain concentration matrices[1] $\boldsymbol{A}^{(\beta\gamma)}$, which connect the subcell and average strains, and the vector $\boldsymbol{D}^{(\beta\gamma)}$, which contains information on thermal and plastic deformation in the $(\beta\gamma)$ subcell of the (q, r) cell. The localization relations have the form

$$\left[\bar{\varepsilon}^{(\beta\gamma)}\right]^{(q,r)} = \left[\boldsymbol{A}^{(\beta\gamma)}\bar{\varepsilon} + \boldsymbol{D}^{(\beta\gamma)}\right]^{(q,r)} \tag{12}$$

Use of these relations in the expression for the average composite stress given in terms of the volume-average subcell stresses, in conjunction with the volume-averaged subcell stress–strain equations, leads to the macroscopic constitutive equation for the multiphase composite in the form

$$\bar{\boldsymbol{\sigma}} = \boldsymbol{C}^{*}\bar{\varepsilon} - (\bar{\boldsymbol{\sigma}}^{I} + \bar{\boldsymbol{\sigma}}^{T}) \tag{13}$$

where the homogenized stiffness matrix for the composite is given in terms of the subcell geometry, material properties, and the elastic Hill strain concentration matrices,

$$\boldsymbol{C}^{*} = \frac{1}{HL}\sum_{q=1}^{N_q}\sum_{r=1}^{N_r}\sum_{\beta,\gamma=1}^{2} h_{\beta}^{(q)} l_{\gamma}^{(r)}\left[\boldsymbol{C}^{(\beta\gamma)}\boldsymbol{A}^{(\beta\gamma)}\right]^{(q,r)} \tag{14}$$

and the inelastic and thermal terms are given in terms of the corresponding quantities

$$\bar{\boldsymbol{\sigma}}^{I} + \bar{\boldsymbol{\sigma}}^{T} = \frac{-1}{HL}\sum_{q=1}^{N_q}\sum_{r=1}^{N_r}\sum_{\beta,\gamma=1}^{2} h_{\beta}^{(q)} l_{\gamma}^{(r)}\left[\boldsymbol{C}^{(\beta\gamma)} - \boldsymbol{D}^{(\beta\gamma)} - \boldsymbol{R}_{(0,0)}^{(\beta\gamma)} - \boldsymbol{\Gamma}^{(\beta\gamma)}\Delta T\right]^{(q,r)} \tag{15}$$

Classical Plasticity Model for the Phases

In the present study, the inelastic response of the matrix phase in the investigated unidirectional metal matrix composites was modeled using the classical incremental plasticity theory. Mendelson's method of successive iterations,[10] described briefly later, and in more detail elsewhere, is employed to solve Eq. (9) for the unknown coefficients $W_{i(mn)}^{(\beta\gamma)}$ and the plastic strain distributions $\varepsilon_{kl}^{p(\beta\gamma)}$ in the individual subcells at each applied load increment, from which the localization relations necessary in the calculation of the macroscopic response are determined. Toward this end, the plastic strain field in the $(\beta\gamma)$ subcell at the current macroscopic strain is expressed in terms of the known initial distribution from the preceding loading state plus an increment that results from the imposed strain increment,

$$\varepsilon_{kl}^{p(\beta\gamma)}\left(\bar{y}_2^{(\beta)}, \bar{y}_3^{(\gamma)}\right)\Big|_{\text{current}} = \varepsilon_{kl}^{p(\beta\gamma)}\left(\bar{y}_2^{(\beta)}, \bar{y}_3^{(\gamma)}\right)\Big|_{\text{previous}} + d\varepsilon_{kl}^{p(\beta\gamma)}\left(\bar{y}_2^{(\beta)}, \bar{y}_3^{(\gamma)}\right) \tag{16}$$

The plastic increments at the individual locations within the subcell are obtained from the Prandtl–Reuss flow rule expressed in terms of Mendelson's modified total strain deviators e'_{ij}, rather than deviatoric stresses, as follows [omitting the subcell designation $(\beta\gamma)$ for notational clarity]:

$$d\varepsilon_{ij}^{p} = (e'_{ij}/\bar{e}_{\text{eff}})d\bar{\varepsilon}^{p} \tag{17}$$

where $e'_{ij} = \varepsilon_{ij} - 1/3\varepsilon_{kk}\delta_{ij} - \varepsilon_{ij}^{p}\big|_{\text{previous}}$ and $\bar{e}_{\text{eff}} = \sqrt{2/3e'_{ij}e'_{ij}}$ and the effective plastic strain increment $d\bar{\varepsilon}^{p}$ is given by

$$d\bar{\varepsilon}^{p} = \bar{e}_{\text{eff}} - \bar{\sigma}_{\text{eff}}/3\mu \tag{18}$$

In this study, we take the elastoplastic response of the matrix phase, characterized by isotropic hardening, to be bilinear, with the effective stress $\bar{\sigma}_{\text{eff}}$ given by

$$\bar{\sigma}_{\text{eff}}(\bar{\varepsilon}^{p}) = \sigma_y + H_p\bar{\varepsilon}^{p} \tag{19}$$

where σ_y is the yield stress in pure tension and H_p is the slope of the effective stress–plastic strain curve, related to the secondary modulus E_s in the bilinear stress–strain representation of the elastoplastic response as

$$H_p = EE_s/(E - E_s) \tag{20}$$

As already demonstrated, the preceding form of the incremental plasticity equations is completely equivalent to the classical formulation, but possesses the added advantage of producing very quick convergence when used in conjunction with Mendelson's iterative scheme for the solution of Eq. (9). The implementation of these equations is facilitated by the following loading condition for plastic loading:

$$1 - \bar{\sigma}_{\text{eff}}/3\mu\bar{e}_{\text{eff}} \tag{21}$$

shown previously to produce very fast convergence.[11]

Shear Coupling Effect

In this section, we briefly demonstrate the model's predictive capability under transverse loading through comparison with the finite element results generated using the commercial program ANSYS to show the importance of the shear coupling effect. This effect is even more important in composites with locally irregular reinforcement as demonstrated in the following section.

We consider a unidirectional graphite/aluminum composite with 5 and 25% fiber content and a square fiber array. The properties of the individual constituents are given in Tables 1 and 2. The graphite fiber is transversely isotropic, and the aluminum matrix isotropic and 3.58 times stiffer than the fiber in the loading plane. The secondary modulus E_s of the aluminum matrix appearing in Eq. (20) is 6.16 times smaller than Young's modulus, and the given yield stress initiates yielding under uniaxial loading at a relatively small strain of 0.4%.

For the HFGMC simulations, the RUC for both fiber volume fractions was dscretized into 36×36 subcells to capture the circular fiber shape with high fidelity.[4,5] For the finite element simulations, a refined representation of one-quarter of the RUC containing 1260 elements with 3909 nodes was constructed using 8-noded, plane-strain quadrilateral elements. External loading was specified in the form of uniform displacements of opposite signs but equal magnitudes applied to the right horizontal and top vertical faces of the unit cell under the condition of plane strain in the out-of-plane direction, $\bar{\varepsilon}_{11} = 0$, and symmetry conditions on the remaining faces. This type

Table 1 Elastic moduli of the transversely isotropic graphite fiber

Property	Value
E_A, GPa	388.20
ν_A	0.41
E_T, GPa	7.60
ν_T	0.45
G_A, GPa	14.90

Table 2 Elastic and plastic moduli of the isotropic aluminum matrix

Property	Value
E, GPa	72.40
ν	0.33
G, GPa	27.22
σ_Y, MPa	286.67
E_S, GPa	11.70

of loading represents pure shearing in the coordinate system rotated by 45 deg about the fiber's center and provides a critical test of HFGMC's predictive capability under transverse loading.

Figure 3 provides the comparison between the high-fidelity model and finite element predictions of the macroscopic stress–strain response for the 25% fiber volume composite. There is virtually no difference between the predictions of the two models. The same holds true for the 5% (dilute) case.[4,5] Included in Fig. 3 is the prediction of the original GMC. As observed, the initial elastic response is captured very well by this simpler model despite the inherent absence of shear coupling. The predictive capability of this model is also quite good in the elastoplastic region but does depend on the fiber volume fraction and also the type of applied loading. The reason for GMC's ability to model the macroscopic inelastic response, that is, initial modulus and subsequent average stress–strain behavior, of metal matrix composites with good accuracy under transverse normal (and also axial normal and axial shear) loading is its ability to reproduce the microlevel effective stress responsible for plasticity effects with good accuracy. However, the individual stress components are not always captured sufficiently well by the original GMC model, as will be discussed.

Figure 4 shows the transverse shear stress σ_{23} distributions generated using the high-fidelity model and the finite element analysis for the dilute case at the applied transverse normal strain $\bar{\varepsilon}_{33}$ of 1%. Clearly, the magnitude of the transverse shear stress is significant and cannot be neglected. Comparison of the two sets of predictions reaffirms the predictive capability of the high-fidelity model. In stark contrast, GMC predicts that the transverse shear stress is identically zero, which is a direct consequence of the absence of shear coupling. Apparently, lack of shear coupling, while resulting in poor prediction for local distributions of certain stress components, has little effect on the method's ability to capture accurately the macroscopic behavior for this loading type and square geometry of the RUC. This is not the case for locally irregular periodic materials as discussed in the next section.

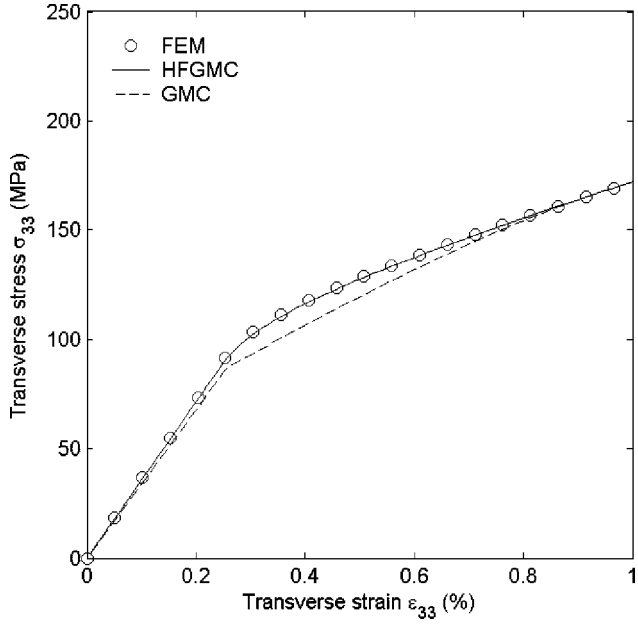

Fig. 3 Macroscopic transverse stress–strain response of a unidirectional graphite/aluminum composite with 25% fiber content under plane strain, $\bar{\varepsilon}_{11} = 0$, biaxial tension–compression, $\bar{\varepsilon}_{22} = -\bar{\varepsilon}_{33}$ loading.

Irregular RUC Response

We consider the inelastic response of a unidirectional boron/aluminum composite with two types of irregular periodic microstructures containing the same fiber content by volume (36%) and compare it with the corresponding composite whose RUC is characterized by a square fiber array shown in Fig. 5a. Of the two irregular microstructures, one is completely random (Fig. 5b), whereas the remaining one (Fig. 5c), although also apparently random, on closer examination contains fibers preferentially aligned in one direction in the transverse $x_2 - x_3$ plane. This fiber preferential alignment produces a composite with monoclinic symmetry. The material properties of the isotropic elastic boron fibers and the elastoplastic aluminum matrix characterized by isotropic hardening and bilinear stress–strain response are given in Tables 3 and 4. The response of the three fiber microstructures is investigated and compared under transverse normal and shear loading applied in the $x_2 - x_3$ plane. The simulations performed using the new high-fidelity micromechanics model are repeated using the original GMC model for comparison.

The macroscopic stress–strain responses of the three fiber arrays under transverse loading generated using the two models are given in Fig. 6. Both models predict that the composite with the square fiber array produces the stiffest response, followed by the completely random and then monoclinic arrays. The softer response of the random

Table 3 Elastic moduli of the isotropic boron fiber

Property	Value
E, GPa	420.00
ν	0.20
G, GPa	175.00

Table 4 Elastic and plastic moduli of the isotropic aluminum matrix

Property	Value
E, GPa	70.00
ν	0.33
G, GPa	26.32
σ_Y, MPa	250.00
E_S, GPa	10.00

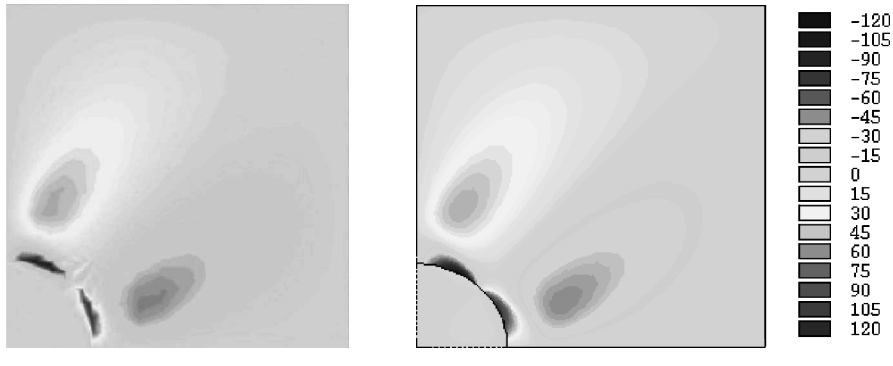

a) High-fidelity GMC **b) Finite element analysis**

Fig. 4 Transverse shear stress σ_{23} fields (megapascal) in a unidirectional graphite/aluminum composite with 5% fiber content at the applied average normal strain $\bar{\varepsilon}_{33}$ of 1.0%.

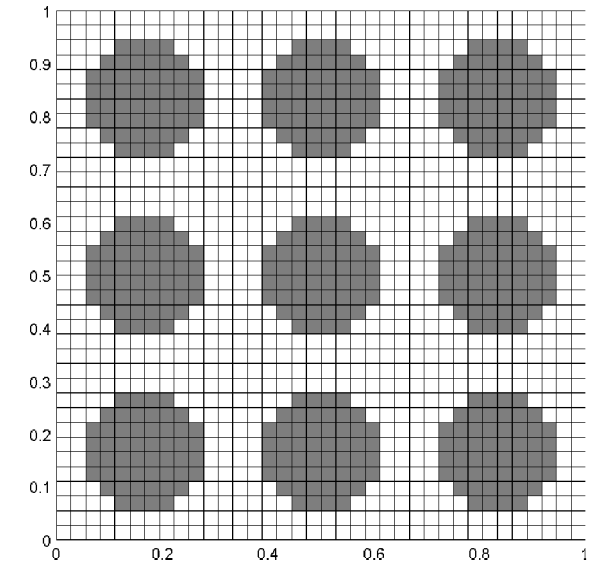

a)

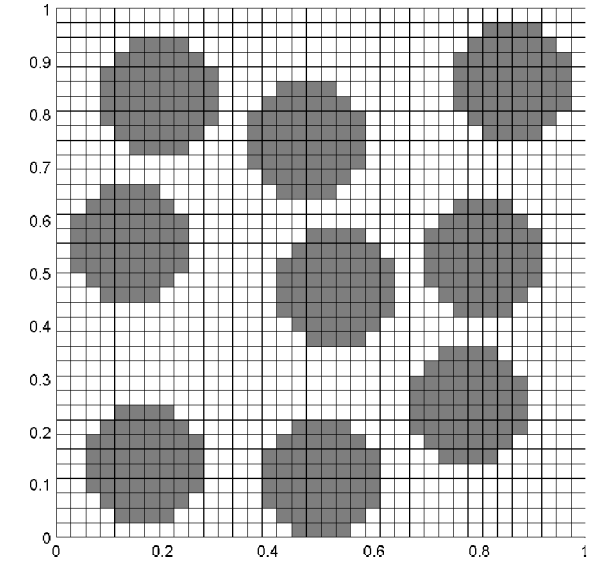

b)

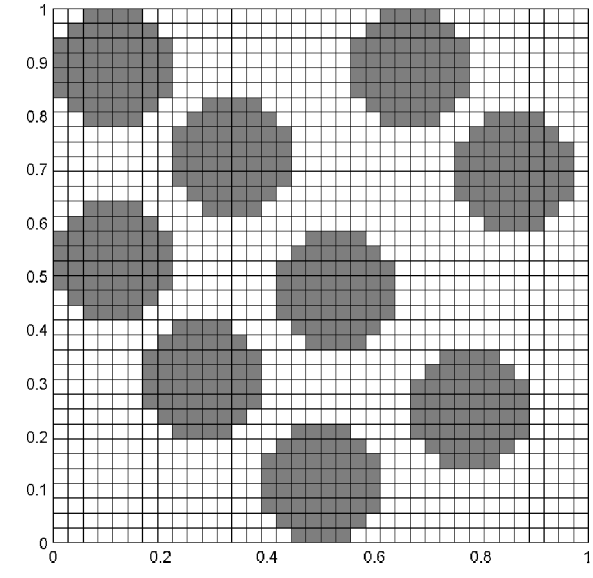

c)

Fig. 5 Investigated boron/aluminum microstructural architectures with 36% fiber content: a) square array, b) irregular array, and c) irregular array with transverse monoclinic symmetry.

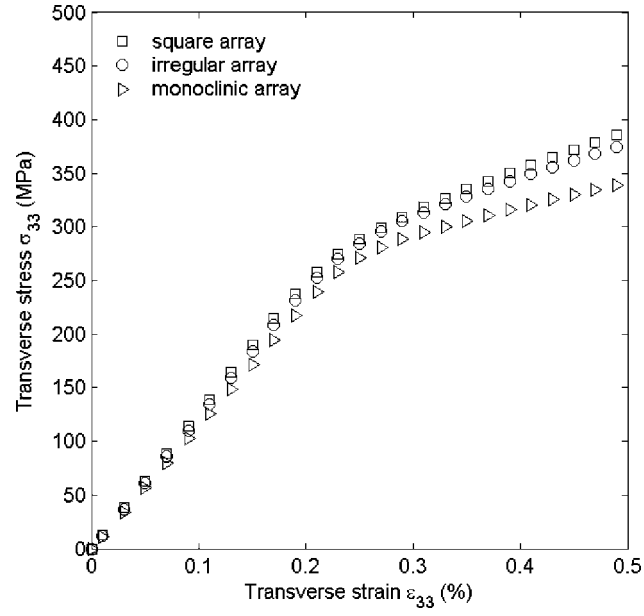

a) High-fidelity GMC

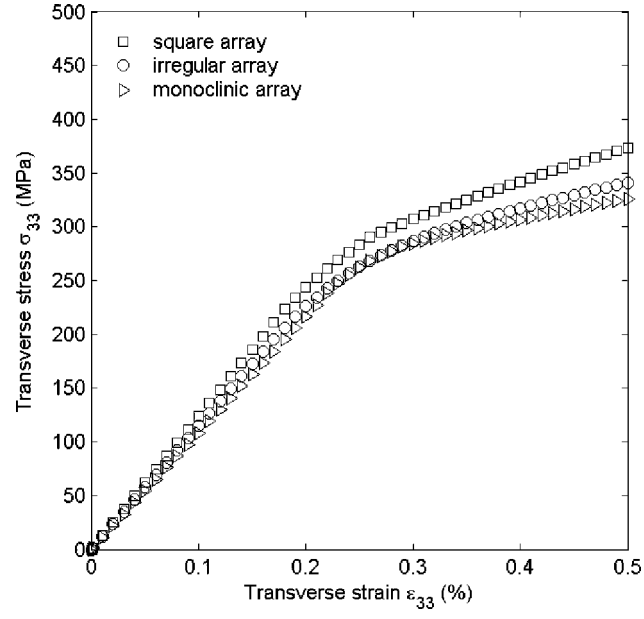

b) Original GMC

Fig. 6 Transverse normal stress–strain response of a boron/aluminum unidirectional composite with three different types of internal microstructure.

array is in agreement with previously reported results generated by the finite element technique.[12–14] The HFGMC model predicts that the differences in the initial elastic moduli and subsequent elastoplastic response are small for the square and completely random arrays. These differences increase with increasing constituent moduli mismatch and fiber volume content. In contrast, the response of the monoclinic array, apparently thus far not investigated, is noticeably more compliant in the elastic region and, to a more pronounced extent, in the plastic region. The predictions of the original GMC model differ from the HFGMC predictions in that the responses of the random and monoclinic arrays are quite close and noticeably lower than the response of the square array.

The reason for the observed differences in the macroscopic responses of the three fiber architectures, as well as the differences in the two models' predictions, can be traced to the local transverse normal stress distributions shown in Fig. 7. As observed, both models indicate that the square fiber array localizes the transverse stress in the matrix separating adjacent fibers along horizontal fiber rows

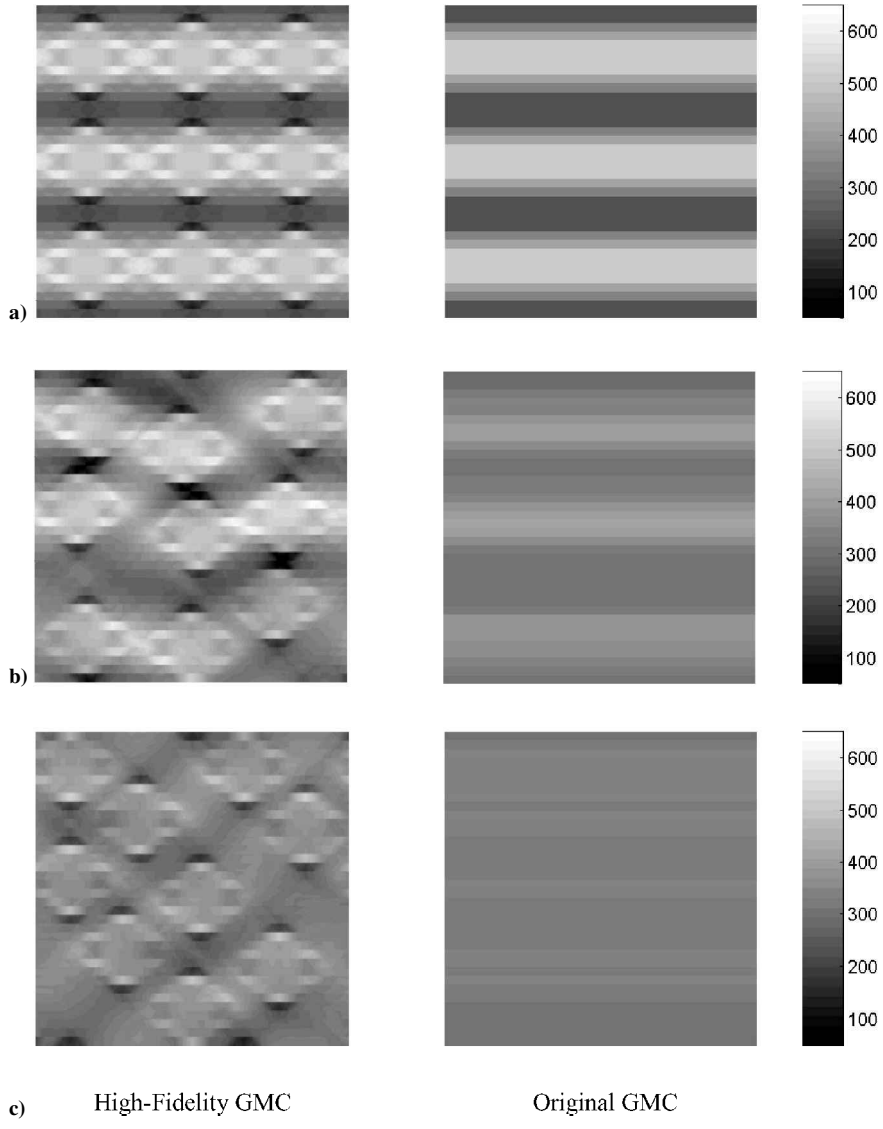

Fig. 7 Transverse normal stress fields (megapascal) in a boron/aluminum unidirectional composite with three different types of internal microstructures at the applied average normal strain of 0.5%: a) square array, b) irregular array, and c) monoclinic array.

lined up with the applied load. The matrix channels between the horizontal fiber rows, on the other hand, experience much lower transverse stress and, consequently, smaller plastic strains. Because the original GMC model uses a first-order displacement field representation at the subcell level, the imposition of traction continuity in a surface-average sense from subcell to subcell along the loading direction produces a transverse stress distribution characterized by constant magnitude strips along this direction. The higher-order displacement field representation in the new model, on the other hand, does produce the expected spatial variation of this traction component along the loading direction due to shear coupling even though traction continuity is also applied in a surface average. Nevertheless, the basic character of the transverse normal stress field is captured by both models in the case of the square array.

The differences in the local transverse stress distributions predicted by the two models, which explain the observed macrolevel trends, are quite apparent in the case of the locally irregular microstrucures. The high-fidelity model predicts that the random microstructure also tends to localize the transverse stress in regions adjacent to the fibers in the direction of the applied load, thereby sheltering the remaining regions of the matrix phase to a certain extent. On the other hand, the matrix phase of the monoclinic array is stressed more uniformly and to a greater extent than in the first two cases, giving rise to more plastic strain and, thus, more compliant macroscopic response. In contrast, the local stress distributions predicted by the original model for these two microstructures exhibit substantially different trends. Although some localization is evident in the random microstructure, the stress magnitudes are much lower than those predicted by the high-fidelity model for this array. The reason for this lies in the absence of shear coupling, which is the primary mechanism from transferring stress from the harder to the softer phase. Whereas no localization is evident in the monoclinic array because the applied load does not see any channels containing only the matrix phase or rows of aligned fibers, the actual stress magnitudes are not substantially different than those seen in the random array. This explains why the original model predicts similar macrolevel responses for the random and monoclinic arrays, in contrast with the high-fidelity model.

The differences between the predictive capability of the two models for locally irregular composites are even more pronounced under shear loading in the $x_2 - x_3$ plane. The macroscopic stress–strain responses for the three fiber arrays under this type of loading generated using the two models are given in Fig. 8. In this case, the microstructure-dependent trend predicted by the high-fidelity model is reversed, with the monoclinic array producing the stiffest response, followed by the irregular and then square array. Furthermore, the relative differences in the responses of the different arrays are more pronounced relative to the normal loading case. In contrast, the original GMC model predicts the same macrolevel transverse shear stress–strain for the three fiber arrays. The differences

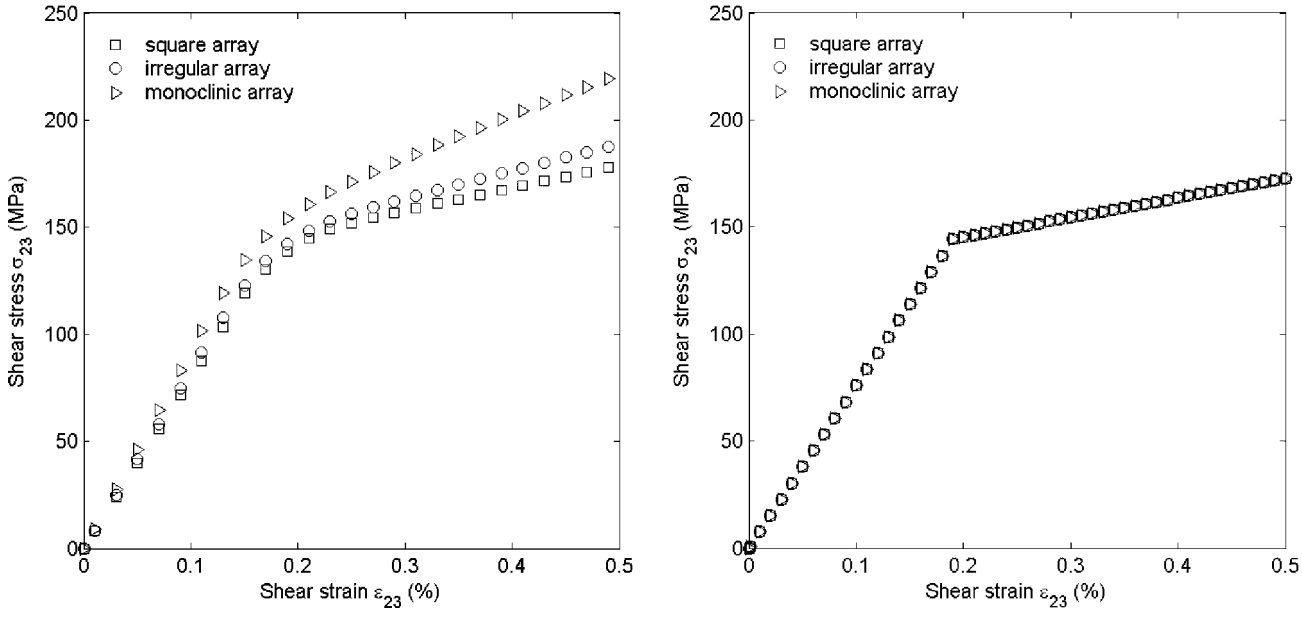

a) High-fidelity GMC **b) Original GMC**

Fig. 8 Transverse shear stress-strain response of a boron/aluminum unidirectional composite with three different types of internal microstructure.

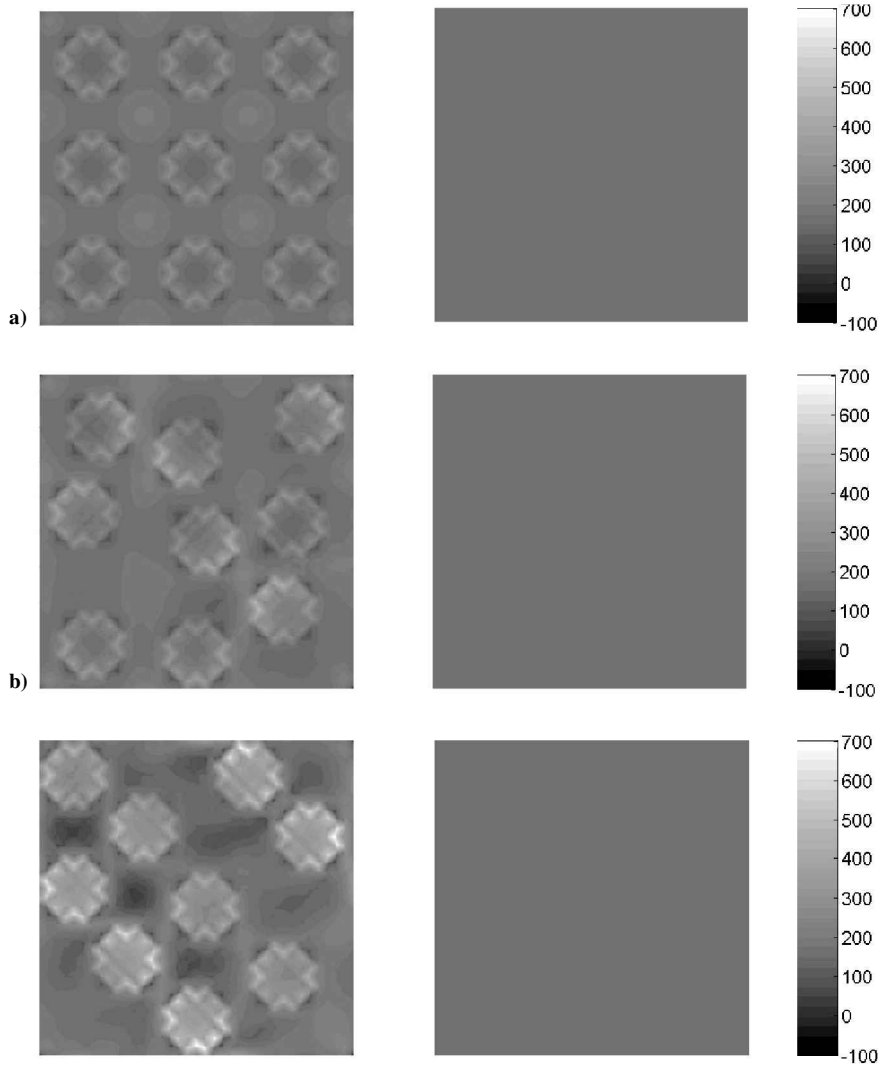

Fig. 9 Shear stress fields (megapascal) in a boron/aluminum unidirectional composite with three different types of internal microstructures at the applied average shear strain of 0.5%: a) square array, b) irregular array, and c) monoclinic array.

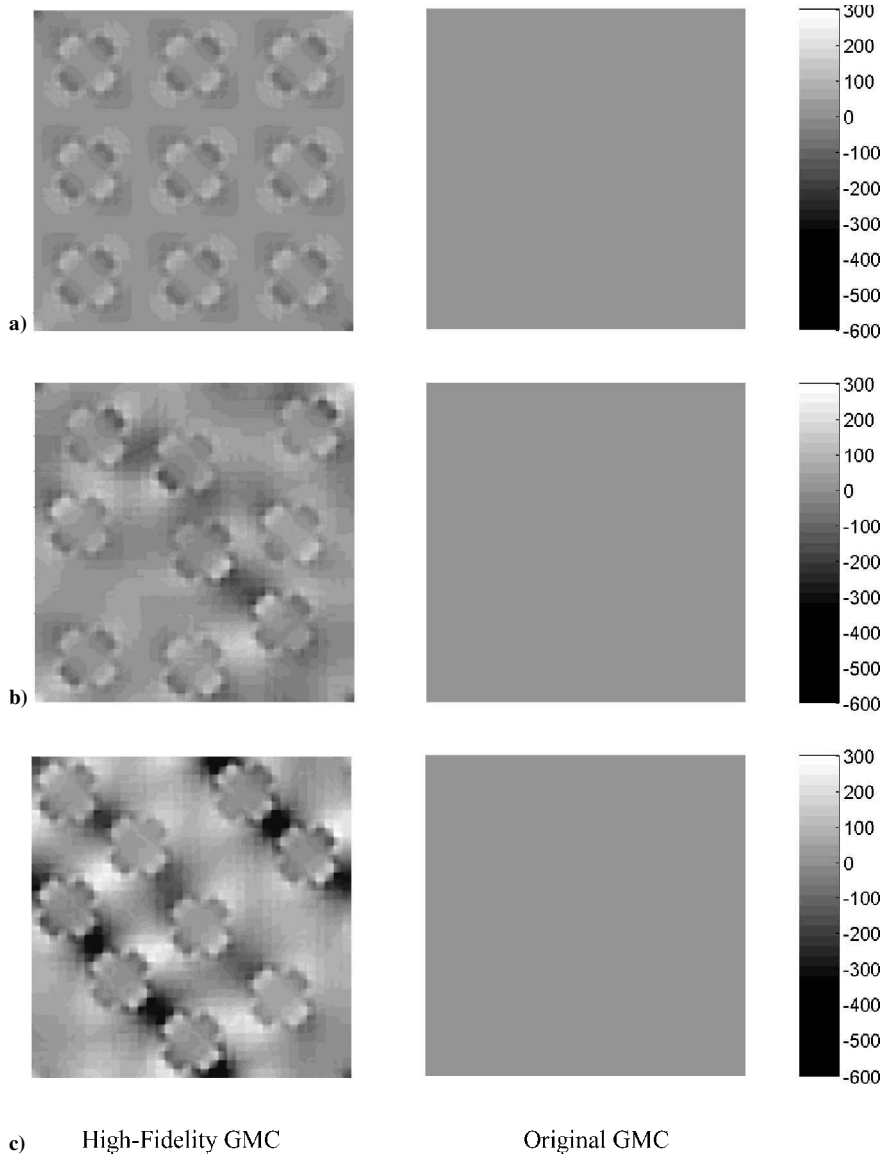

Fig. 10 Hydrostatic stress fields (megapascal) in a boron/aluminum unidirectional composite with three different types of internal microstructures at the applied average shear strain of 0.5%: a) square array, b) irregular array, and c) monoclinic array.

predicted by the high-fidelity model, as well as the absence of differences predicted by the original model, are also explained by the internal stress fields.

Figure 9 presents the local shear stress distributions for the three fiber arrays generated by the two models. The high-fidelity model predicts a substantially higher shear stress in the matrix phase of the square array relative to the monoclinic array (where sign reversal is also observed), thus, resulting in the most compliant response. The mononclic array localizes the shear stress within the elastic fibers, while lowering this stress component in the matrix phase to the extent that changes in the shear stress sign occur in some matrix regions, thus, producing the stiffest macroscopic response of the three arrays. The internal shear stress magnitudes in the random array are only somewhat lower than in the regular array, producing a somewhat stiffer response. In contrast, the original GMC model predicts identical shear stress fields for the three different architectures. This is a direct result of the first-order displacement field approximation in the individual subcells, which produces piecewise uniform subcell stress fields and, thus, a uniform full-field transverse shear stress field due to the application of traction continuity in an average sense in the presence of macroscopically uniform loading.

Additional insight into the observed differences in the macroscopic shear stress–strain responses of the three arrays predicted by the high-fidelity model, and the inability of the original model to capture these differences, is gained by examining the local effective and hydrostatic stress distributions. The effective stress is directly responsible for plastic flow in the matrix phase, whereas the hydrostatic stress prevents the evolution of plastic flow. Examination of the effective stress distributions in the three fiber architectures, not shown here because their character is similar to the shear stress distributions shown in Fig. 9, indicates that the effective stress in the matrix phase of the monoclinic array predicted by the high-fidelity model is smaller relative to the square and random arrays. The smaller values of the effective stress in the matrix phase are offset by the higher values in the fibers. The lower magnitudes of the matrix effective stress in the monoclinic array are accompanied by the higher magnitudes of the corresponding hydrostatic stress relative to the other two arrays, shown in Fig. 10. This provides additional evidence for the stiffer response of the monoclinic array under shear loading relative to the square and random arrays.

In contrast, the original GMC model predicts the same uniform distributions of the effective stress throughout the entire repeating unit cell for the three different arrays and complete absence of the hydrostatic stress. This is a direct result of the lack of shear coupling, which produces a state of stress throughout the entire RUC characterized by just one component, namely, the transverse shear stress component, whose magnitude is identical to the macroscopic value.

Conclusions

The recently developed micromechanics model HFGMC has been demonstrated to be capable of predicting the response of periodic composites with locally irregular fiber distributions. Prior investigations of the model's predictive capability were limited to periodic composites characterized by RUCs with orthogonal planes of material symmetry. The results presented herein have demonstrated the model's wider range of applicability to periodic multiphase materials without easily definable planes of material symmetry. Local irregularities in reinforcement phase distribution may arise naturally due to a particular fabrication process or may be introduced deliberately to alter the material response. The presented examples clearly demonstrate the model's sensitivity in capturing the macroscopic response and the local stress fields that are influenced by the changes in the reinforcement phase distribution. This capability is a direct consequence of the shear coupling effect that is an inherent feature of the new model. This effect is rooted in the use of a higher-order displacement field approximation within the individual phases of the heterogeneous material relative to that employed in the simpler GMC model from which HFGMC evolved, which is incapable of correctly predicting the observed trends due to the lack of shear coupling.

The specific examples presented have demonstrated an interesting influence of two particular random fiber distributions on the normal and shear response of a metal matrix composite in the plane transverse to the fiber direction. This influence is more pronounced for shear loading, and clearly demonstrates the importance of the shear coupling effect, and, thus, the significance of the high-fidelity model.

Acknowledgment

The support of NASA John H. Glenn Research Center at Lewis Field through Grant NAG3-2524 is gratefully acknowledged.

References

[1]Hill, R., "Elastic Properties of Reinforced Solids: Some Theoretical Principles," *Journal of the Mechanics and Physics of Solids*, Vol. 11, 1963, pp. 357–372.

[2]Kalamkarov, A. L., and Kolpakov, A. G., *Analysis, Design and Optimization of Composite Structures*, Wiley, New York, 1997, pp. 3–44.

[3]Aboudi, J., Pindera, M. J., and Arnold, S. M., "Linear Thermoelastic Higher-Order Theory for Periodic Multiphase Materials," *Journal of Applied Mechanics*, Vol. 68, No. 5, 2001, pp. 697–707.

[4]Aboudi, J., Pindera, M.-J., and Arnold, S. M., "High-Fidelity Generalized Method of Cells for Inelastic Periodic Multiphase Materials," NASA TM 2002-211469, March 2002.

[5]Aboudi, J., Pindera, M.-J., and Arnold, S. M., "Higher-Order Theory for Periodic Multiphase Materials with Inelastic Phases," *International Journal of Plasticity*, Vol. 19, No. 6, 2003, pp. 805–847.

[6]Aboudi, J., Pindera, M.-J., and Arnold, S. M., "Higher-Order Theory for Functionally Graded Materials," *Composites: Part B*, Vol. 30, No. 8, 1999, pp. 777–832.

[7]Paley, M., and Aboudi, J., "Micromechanical Analysis of Composites by the Generalized Method of Cells," *Mechanics of Materials*, Vol. 14, 1992, pp. 127–139.

[8]Orozco, C., "Computational Aspects of Modeling Complex Microstructure Composites with GMC," *Composites: Part B*, Vol. 28, No. 1-2, 1997, pp. 167–175.

[9]Orozco, C., and Pindera, M.-J., "Plastic Analysis of Complex Microstructure Composites Using the Generalized Method of Cells," *AIAA Journal*, Vol. 37, No. 4, 1999, pp. 482–488.

[10]Mendelson, A., *Plasticity: Theory and Application*, reprint ed., Krieger, Malabar, FL, 1986, pp. 164–171.

[11]Williams, T. O., and Pindera, M. J., "An Analytical Model for the Inelastic Axial Shear Response of Unidirectional Metal Matrix Composites," *International Journal of Plasticity*, Vol. 13, No. 3, 1997, pp. 261–289.

[12]Brockenbrough, J. R., and Suresh, S., "Plastic Deformation of Continuous Fiber-Reinforced Metal-Matrix Composites: Effects of Fiber Shape and Distribution," *Scripta Metallurgica and Materialia*, Vol. 24, 1990, pp. 325–330.

[13]Brockenbrough, J. R., Suresh, S., and Wienecke, H. A., "Deformation of Metal-Matrix Composites with Continuous Fibers: Geometric Effects of Fiber Distribution and Shape," *Acta Metallurgica and Materialia*, Vol. 39, No. 5, 1991, pp. 735–752.

[14]Arnold, S. M., Pindera, M.-J., and Wilt, T. E., "Influence of Fiber Architecture on the Inelastic Response of Metal Matrix Composites," *International Journal of Plasticity*, Vol. 12, No. 4, 1996, pp. 507–545.

A. Palazotto
Associate Editor